Semi-Automated Segmentation of Symptomatic Exudate-Associated Derangements (SEADs) in 3D OCT Using Layer Segmentation

Martin Dolejší[1], Michael D. Abràmoff[2], Milan Sonka[3], Jan Kybic[1]
[1]Center for Machine Perception, CTU, Prague, Czech Republic, [2]Dpt of Ophthalmology and Visual Sciences, University of Iowa Hospitals and Clinics, USA, [3]Dpt of Electrical and Computer Engineering, University of Iowa, USA
dolejm1@fel.cvut.cz

Abstract. We present a novel two step method to segment retinal pathologies related to the so called wet age-related macular degeneration from 3D spectral optical coherence tomography images. In the first step we segment three retinal layers by an optimal surface algorithm. The identified layers are used in the second step to constrain the segmentation of fluid filled retinal regions using GraphCut. We propose a new regularization energy term for GraphCut that permits long range effect of the manual initialization.

1 Introduction

The Age-related macular degeneration (AMD) is a disease associated with aging that gradually destroys sharp central vision. A 'wet' version of AMD exhibits lesions called symptomatic exudate-associated derangements (SEADs). The treatment for wet AMD is available [1], but will only reach its full potential when objective measures of treatment response are developed.

The aim of this work is to develop an algorithm to segment SEADs in 3D optical coherence tomography (3D OCT) images, as today manual segmentation is used [2]. There is also an automatic segmentation tool [3], but it fails on more than 30% of testing scans [3].

2 Methods

For constrained multiple layer segmentation (first step) we adopted the optimal surface approach [4]. This approach is based on finding an optimal closed set (subset of nodes, such that all successors of any node in the closed set are also contained in the closed set) in an oriented node-weighted graph and is capable to segment terrain-like surfaces. The surfaces are globally optimal in the sense of a given cost function. The cost of surfaces is defined as the total cost of all nodes laying on the surfaces:

$$E = \sum_{s=1}^{S} \sum_{\forall n_i \in \mathcal{N}_s} c_s(n_i) \ , \tag{1}$$

where $\mathcal{N}_s$ is set of s-th surface nodes and $c_s(n_i)$ is cost of i-th node on s-th surface. As the node cost we use the z-axe gradient obtained by applying gradient filter $k_g = [1, -1]$ and 26-neighbourhood averaging filter k_s. We use dark→light gradient for two upper layers, light→dark gradient for third and booth gradients for the bottom one:

$$c_s = \begin{cases} f * k *_g * k_s & \text{for upper two surfaces} \\ -f * k_g * k_s & \text{for third surface} \\ |f * k_g * k_s| & \text{for bottom surface} \ , \end{cases} \tag{2}$$

where f is image function and $*$ stands for convolution.

Once we have identified the layer boundaries, we will find the SEADs using GraphCut (second step) as described below. The segmentation uses a set of manually selected foreground and

background voxels, $\mathcal{C}_b$ and $\mathcal{C}_f$. Let the 3D image be represented by a graph $\mathcal{G} = \langle \mathcal{V}, \mathcal{E} \rangle$. Each vertex $v \in \mathcal{V}$ represents a voxel and there is an intensity function $f : \mathcal{V} \to I = \{0 \dots 255\}$. All adjacent voxels in 6-connectivity are linked by an edge $e \in \mathcal{E}$. Two class segmentation $s \in \mathcal{S}$ is defined as $s\colon \mathcal{V} \to \{0, 1\}$, with 0 meaning background and 1 foreground. The objective function of the graph-based segmentation is:

$$E_a(s, f, \mathcal{C}_b, \mathcal{C}_f) = a_1 \sum_{\substack{\forall e \in \mathcal{E}, \\ e=\{k,k'\}}} -\delta\big(s(k), s(k')\big) \log g\big(f(k), f(k')\big) + \\ + a_2 \sum_{\forall k \in \mathcal{V}} \log h(s(k), \mathcal{C}_b, \mathcal{C}_f) + a_3 \prod_{\forall k \in \mathcal{V}} -\log p\big(f(k)|s(k)\big) \ . \tag{3}$$

The first term is used for regularization, penalizing adjacent pixels being classified differently, unless their intensity difference (measured by g) is small. The Kronecker delta is defined as:

$$\delta\big(s(k), s(k')\big) = \begin{cases} 0 & \text{if } s(k) = s(k') \\ 1 & \text{otherwise.} \end{cases} \tag{4}$$

The regularization weights $\log g$ are derived from the voxel contrast using a piecewise linear mapping function:

$$g\big(f(k), f(k')\big) = \begin{cases} \epsilon & \text{if } m < \alpha m^* \\ (1-\alpha)m + \epsilon & \text{if } \alpha m^* \le m < \beta m^* \\ \beta m^* - \alpha m^* + \epsilon & \text{if } \beta m^* \le m \ , \end{cases} \tag{5}$$

where

$$m = \big|f(k) - f(k')\big|, \tag{6}$$

and

$$m^* = \max_{\substack{\forall e \in \mathcal{E}, \\ e=\{l,l'\}}} \big|f(l) - f(l')\big| \ . \tag{7}$$

The second term of Eq. (3) is novel. It uses a distance from the current point k to the nearest foreground or background initialization point:

$$\begin{aligned} h(s(k), \mathcal{C}_b, \mathcal{C}_f) \ &= \ s(k) \min_{\forall c_f \in \mathcal{C}_f} \|k - c_f\| + \\ &+ \ \big(1 - s(k)\big) \min_{\forall c_b \in \mathcal{C}_b} \|k - c_b\| \ . \end{aligned} \tag{8}$$

Notation $\|k - c_x\|$ stands for Euclidean distance of voxels represented by vertices k and c_x.

The third part of the energy function (3) is the data term, a log-likelihood which can be further expanded:

$$p\big(f(k)|s(k)\big) = s(k) p_f\big(f(k)\big) + \big(1 - s(k)\big) p_b\big(f(k)\big) \ , \tag{9}$$

where p_f and p_b are probabilities of a voxel with intensity $f(k)$ being foreground or background, respectively. We estimate densities p_f and p_b for the current layer separately using a histogram constructed from the 6-neighborhood of all $\mathcal{C}_b$ and $\mathcal{C}_f$ voxels.

To constrain the SEAD to the current layer, we set $p_b = 1$ and $p_f = 0$ for all nodes outside currently processed layer.

The minimizing task:

$$s^* = \operatorname*{argmin}_{\forall s \in \mathcal{S}} E_a(s, f, \mathcal{C}_b, \mathcal{C}_f) \ . \tag{10}$$

is solved using a conventional GraphCut (maximum flow) algorithm [5].

We use a simple graphical user interface (GUI) for incremental manual initialization (defining $\mathcal{C}_b, \mathcal{C}_f$) of the segmentation algorithm, and visualization of the resulting region.

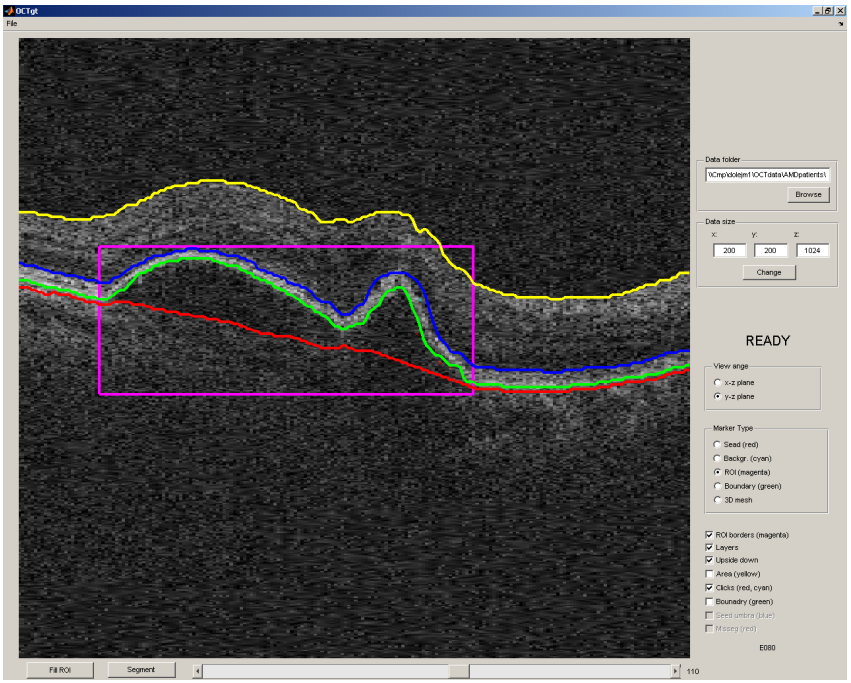

Fig. 1: Screen shot of the interface

3 Experimental methods and results

We used 25 OCT scans of AMD patients for evaluation of our method. The dataset contained 15 eyes, 10 of them were scanned twice within a short time interval. Because there were no ground truth segmentations, we asked two trained operators to segment SEADs in our dataset using our previous approach, which uses GraphCut similarly to what was described here but does not segment the layers first and does not use the layer information. The segmentations obtained by this approach were not accurate (see the first two rows of Figure 2), so we decided to base our evaluation on a clinically significant measurement of SEAD severity independent of SEAD location and shape—the total SEAD volume V [mm^3]. Volume is often used [2] to describe neovascular AMD. Our volumetric measurements between scan pairs (using the old method and images of the same eye) show a nice correlation $\rho = 0.97$, $p_{val} = 2.78.10^{-6}$. For further comparison we averaged the volume from first and second observers' segmentations and call such volumes a 'bronze standard'. Examples of SEAD segmentations as well as the first and second observers' segmentations are in Figure 2.

Our new method produces similar V as the bronze standard, with mean error $\mu_{ns} = 0.25 \pm 0.4$mm^3 (the mean volume is 0.89mm^3); you can see a scatter plot in Figure 3. In Figure 4b we have sorted the results of our 25 experiments by the volume estimation error and we show this error as a function of the relative rank.

We also investigated the reproducibility of our new approach by comparing the segmentation results on the image pairs of the same eye: the mean volume difference for the new method was $\mu_n = 0.12 \pm 0.2$mm^3, while for the bronze standard $\mu_s = 0.16 \pm 0.2$mm^3. Again, we see that the new method is more stable.

The main advantage of the new method is that the number of initialization points needed is much smaller than for the old method. The mean number of initialization points per scan decreased from 216 or 201 for the first or second observer respectively to 12.8 for the new method, which is quite a dramatic reduction that translates into significant time savings. You can see the detailed results in Figure 4a.

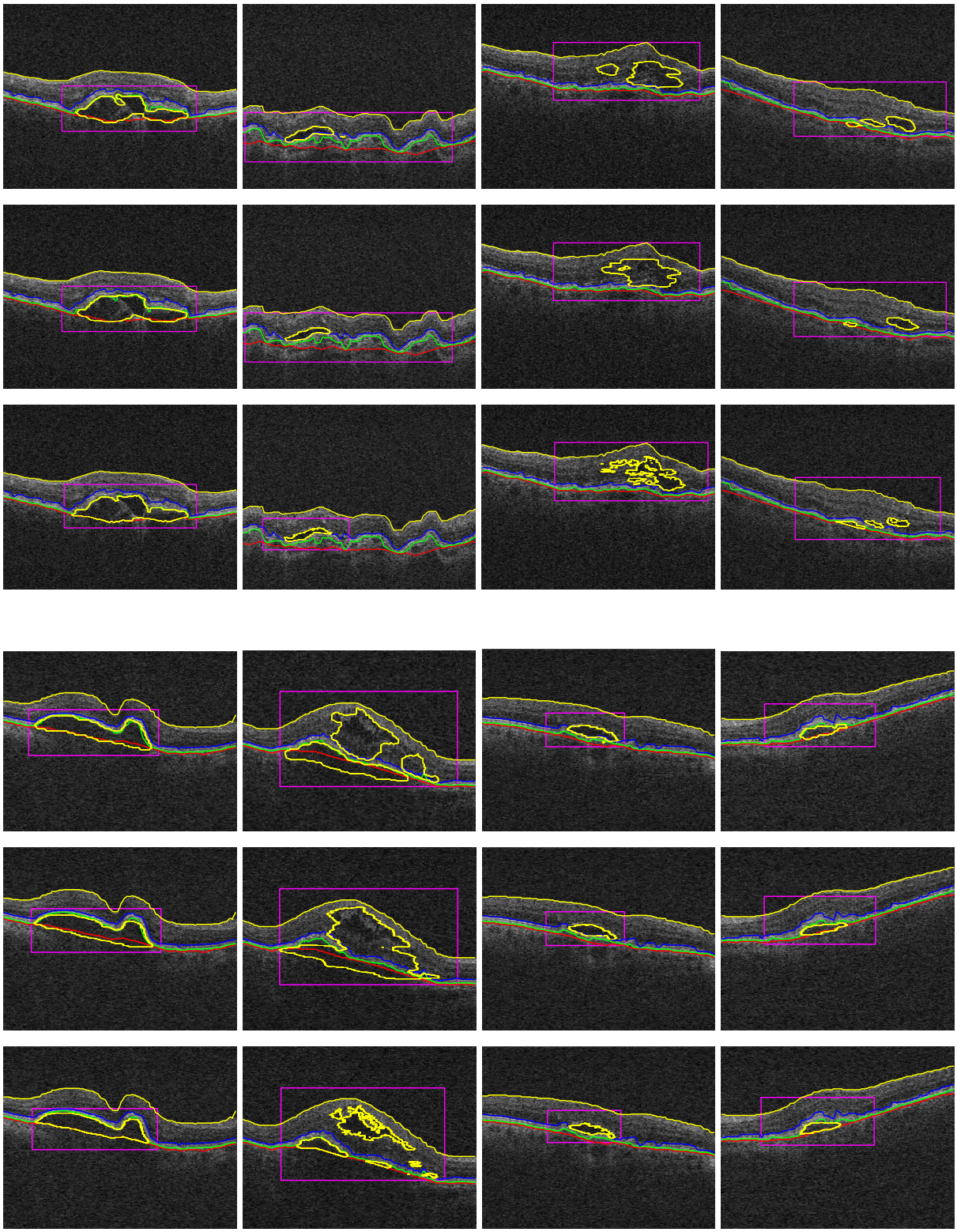

Fig. 2: Examples of eight different SEAD segmentation (marked by thick yellow line). Three different segmentations are shown. From top down: the first and second observer using the old method, and the new method. For better orientation the segmented layer interfaces are also shown (thick red, green, blue, and yellow lines). Note the difficulties of SEAD segmentation in the top layer, where the contrast is low and SEADs irregular, and around the botom interface, where there is almost no contrast.

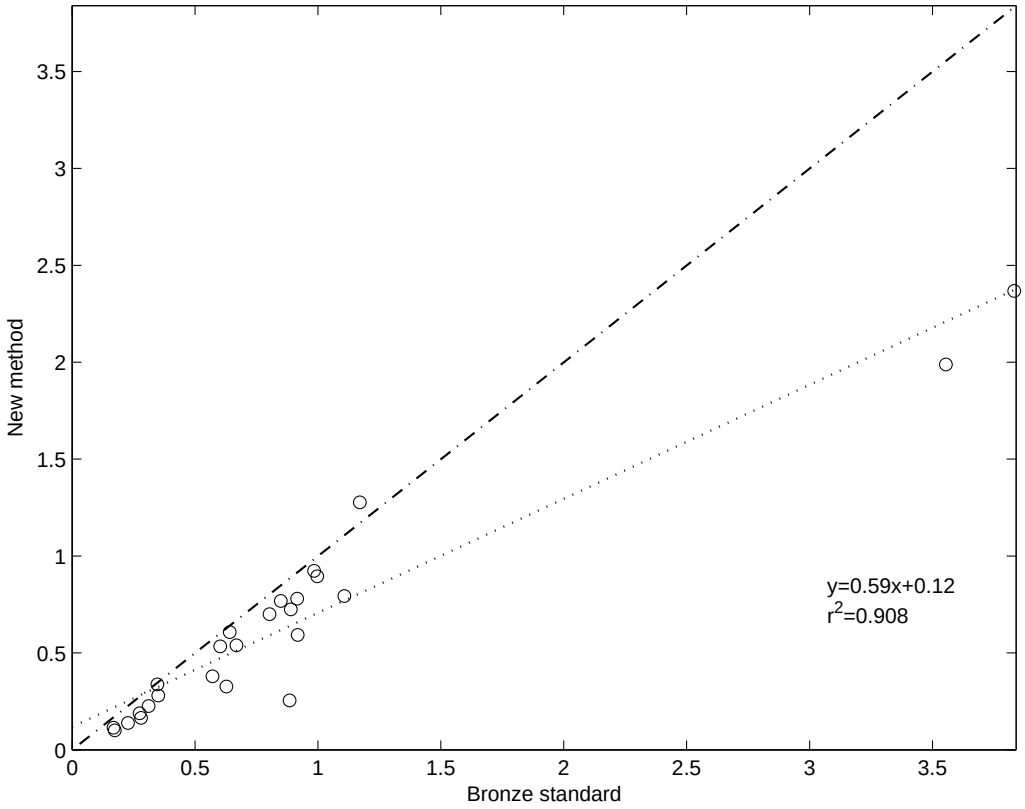

Fig. 3: Volume of the SEADs segmented by the new method with respect to the bronze standard (dash-dotted line: $y = x$, dotted line: $y = 0.6x + 0.1$ least squares linear fit of the data).

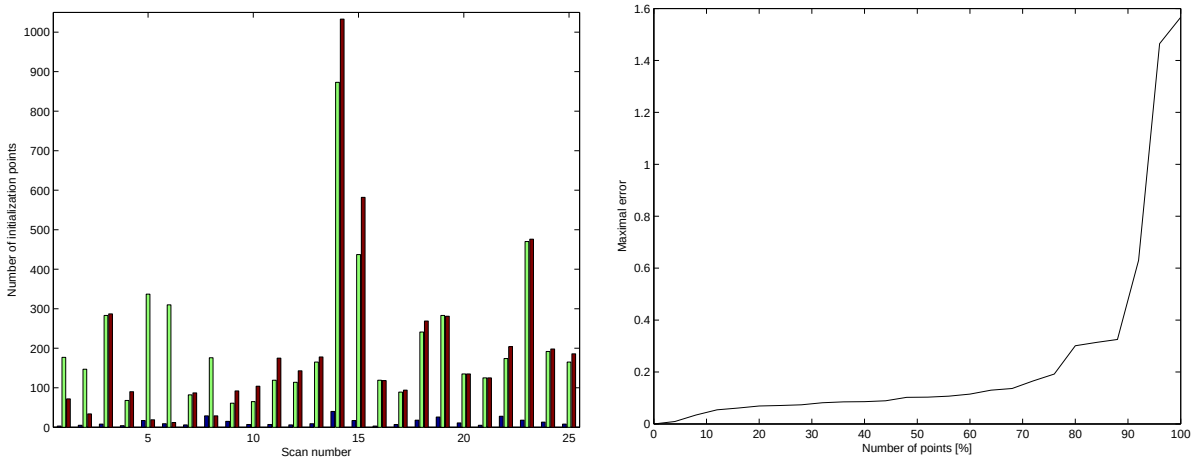

(a) (b)

Fig. 4: Maximum error as a function of the relative rank (a). Number of initialization points. Blue—new method; Red—old method, first expert; Green—old method, second expert (b).

4 Conclusions

We show that introducing the layer segmentation constraints can reduce the number of initialization points necessary for the segmentation of SEADs in 3D OCT images. The segmented volume is consistent with results obtained by two trained operators. This is an important step on the way to a fully automatic SEAD segmenting algorithm. In the future work, we will collect gold standard expert segmentations for a more complete method evaluation.

Acknowledgement

This work has been partly supported by Czech Science Foundation Project 102/07/1317, Czech Ministry of Education project MSM6840770012, NIH NIBIB R01-EB004640 and NIH NEI R01-EY018853, as well as by Research to Prevent Blindness and the U.S. Department of Veterans Affairs.

References

[1] R. F. Spaide, K. Laud, H. F. Fine, J. M. J. Klancnik, C. B. Meyerle, L. A. Yannuzzi, J. Sorenson, J. Slakter, Y. L. Fisher, and M. J. Cooney, "Intravitreal bevacizumab treatment of choroidal neovascularization secondary to age-related macular degeneration," *Retina*, vol. 26, no. 4, pp. 383–390, 2006.

[2] P. A. Keane, S. Liakopoulos, S. C. Ongchin, F. M. Heussen, S. Msutta, K. T. Chang, A. C. Walsh, and S. R. Sadda, "Quantitative subanalysis of optical coherence tomography after treatment with ranibizumab for neovascular age-related macular degeneration," *Investigative Ophthalmology & Visual Science*, vol. 49, no. 7, pp. 3115–3120, July 2008.

[3] C. Ahlers, C. Simader, W. Geitzenauer, G. Stock, P. Stetson, S. Dastmalchi, and U. Schmidt-Erfurth, "Automatic segmentation in three-dimensional analysis of fibrovascular pigmentepithelial detachment using high-definition optical coherence tomography," *British Journal of Ophthalmology*, vol. 92, no. 2, pp. 197–203, February 2008.

[4] K. Li, X. Wu, D. Z. Chen, and M. Sonka, "Optimal surface segmentation in volumetric images—A graph-theoretic approach," *IEEE Transactions on Pattern Analysis and Machine Intelligence*, vol. 28, no. 1, pp. 119–134, 2006.

[5] Y. Boykov and V. Kolmogorov, "An experimental comparison of min-cut/max-flow algorithms for energy minimization in vision," *IEEE Transactions on Pattern Analysis and Machine Intelligence*, vol. 26, no. 9, pp. 1124–1137, 2004.